Mesenchymal stem cell models reveal critical role of Myc as early molecular event in osteosarcomagenesis

Rania Akkawi[1], Judith Diment[2], Gary S. Stein[3], Rami I. Aqeilan[1]

[1]The Concern Foundation Laboratories, The Lautenberg Center for Immunology and Cancer Research, Department of Immunology and Cancer Research-IMRIC, Faculty of Medicine, The Hebrew University of Jerusalem, Jerusalem, Israel; [2]Department of Pathology, Hadassah University Medical Center, Jerusalem, Israel; [3]Department of Biochemistry, College of Medicine, UVM Cancer Center, University of Vermont, Burlington, VT, USA.

*Corresponding author: ramiaq@mail.huji.ac.il

Keywords: MSCs, p53, WWOX, Myc, osteosarcoma

Conflict of Interest: non

Abstract

Osteosarcoma (OS) is an aggressive bone tumor that primarily affects children and adolescents. This malignant tumor is highly aggressive, associated with poor clinical outcomes, and metastasizes mainly to the lungs. Due to its rarity and biological heterogeneity, limited studies of its molecular basis exist, thus hindering the development of effective therapies. WW domain-containing oxidoreductase (WWOX) spans one of the most active and common fragile sites that is frequently altered in human OS. The combined deletion of *Wwox* and *Trp53* using *Osterix1-Cre* transgenic mice has been shown to accelerate OS development. In this study, we generated a traceable OS mouse model, SKO-*Trp53* or DKO-*Wwox*/*Trp53,* expressing a *tdTomato* reporter. By tracking tomato expression at different time points, we detected the early presence of tdTomato-positive cells in the bone marrow (BM) mesenchymal stem cells (MSCs) of non-OS bearing mice, young BM (yBM). We found that DKO yBM cells, but not SKO yBM cells, exhibited tumorigenic traits both *in vitro* and *in vivo*. Molecular and cellular characterization of these DKO yBM cells revealed their resemblance to OS tumor cells. Interestingly, one of the early observed transcriptomic changes in DKO yBM was the upregulation of Myc and its target genes compared to SKO yBM cells. As a prototype target, we further demonstrated the upregulation of MCM7, a known Myc target, in DKO yBM relative to SKO yBM. Therapeutic targeting of MCM7 using simvastatin (SVA) resulted in attenuation of OS tumor growth. Our findings reveal BM-MSCs as a platform to study OS, and reveal Myc and its targets as early molecular events during osteosarcomagenesis.

Introduction

Osteosarcoma (OS) is the most common primary malignant bone tumor that predominantly affects children and adolescents. It often arises in the metaphyses of long bones[1]. OS is highly malignant, with irregular bone growth and distant metastases that are commonly observed in the lungs. The current standards of care for OS are neoadjuvant chemotherapy, surgical resection, and adjuvant chemotherapy. This treatment increases the disease free-survival probability to more than 60% in the localized OS cases[2], but it is still between 10%-40% in metastatic OS[3]. Molecular studies of OS are significantly hindered by its genetic complexity and chromosomal instability [4,5]. In addition, the absence or uncertainty of the exact cell of origin further challenges the identification of therapeutic targets[6]. Therefore, an in-depth molecular understanding of osteosarcomagenesis is urgently needed for better prognosis and management of patients with OS.

WW-domain containing oxidoreductase (WWOX) spans one of the most active common fragile sites of FRA16D[7], and encodes a 46kDa tumor suppressor that is altered in most human cancers[8,9]. We have previously demonstrated that WWOX is frequently altered in human OS and that WWOX restoration in WWOX-negative OS cells suppresses tumorigenicity[10]. Furthermore, our group has shown that ablation of murine *Wwox* using *Osterix1(Osx)-Cre* transgenic mice with a p53-deficient background (DKO) accelerates OS development. DKO tumors display a more aggressive and poorly differentiated phenotype than p53 single KO (SKO) tumors. The DKO model highly recapitulates human OS and represents a valuable platform for investigating OS genetics and preclinical therapeutic targets[11].

Myc is known to be a key player in OS[12,13]. Myc expression regulates several target genes implicated in osteosarcomagenesis. One such example is the minichromosome maintenance proteins (MCMs), which exist in a functional complex consisting of MCM2-7 and play important roles in double-strand DNA unwinding, DNA replication control, and DNA damage repair. Various cancer tissues, including sarcoma and carcinoma cell lines, show overexpression of MCMs, particular MCM7 [14,15,16]. Myc positively regulates MCM7 expression.

Inhibition of MCM7 results in the accumulation of DNA lesions and the activation of the DNA damage checkpoint response, which prevents cells' growth [17]. Interestingly, MCM7 has been shown to be targeted by statins in Rb-deficient tumors[18]. In addition, simvastatin has been shown to suppress tamoxifen-resistant cell growth by inhibiting MCM7 and Rb and subsequently inducing DNA damage[19]. However, the role of statins in the inhibition of MCM7 in OS remains unknown.

Mesenchymal stem cells (MSCs) or osteoblasts can be the cells of origin for OS, although this remains controversial. Research evidence suggests that OS originates during the differentiation process of MSCs into preosteoblast, and that the stage of differentiation affects the OS phenotype and grade [20,21]. In Contrast, others suggest that osteoblast precursor cells are the cells of origin for OS[6,22]. Recently, it was shown that *Osx* is expressed in both the osteoblast lineage (osteoblasts, osteocytes, and chondrocytes) and in bone marrow (BM) stromal cells (MSCs), BM-adipocytes, and BM-perivascular cells[23]. This finding prompted us to use our SKO and DKO models to uncover the early molecular changes in OS development. To this end, we introduced a tdTomato reporter into these models and followed their behavior at different time points. We found that tdTomato-expressing BM isolated from young BM (yBM) DKO mice, prior to OS development, is capable of forming OS tumors that are indistinguishable from DKO tumors. This feature was not observed in the SKO yBM cells. Molecular characterization of yBM DKO cells revealed unique upregulation of Myc expression and its targets at very early stages prior to OS onset. Inhibition of MCM7, a known Myc target, attenuates OS tumor formation. Our model represents a unique platform for studying early changes during osteosarcomagenesis and for assessing vulnerabilities that can be targeted in OS.

Materials and Methods

Mouse strains and tumor models:

The mice were housed in a pathogen-free animal facility at Hebrew University of Jerusalem. To generate our traceable mouse model, we crossed the single knockout (*Trp53*) or double knockout mice (*Wwox*/*Trp53*) Osx1-Cre for deletion of mesenchymal progenitors committed to bone formation[24] with B6.Cg-Gt(ROSA)26SorTm9(CAG-tdTomato) Hze/J (TdT) (catalog #007909; The Jackson Laboratory) to generate SKO-Osx-Cre;tdTomato ($SKO^{TOM)}$ and DKO-Osx-Cre;tdTomato (DKO^{TOM}). Bone Marrow (BM) and tumor cells were collected from mice at different time points.

For Intratibial Injection (IT), 6-8 weeks old NOD/SCID mice were anesthetized with ketamine (80 mg/kg) / xylazine (7 mg/kg) and injected intraperitoneally with 5 mg/kg carprofen. Mice were then injected intratibially with $0.5x10^6$ tumor or BM cultured cells (as explained in BM extraction and cell culture section), suspended in 20µl of sterile complete media (MEM-Alpha (Biological Industries)) supplemented with 10% Fetal Calf Serum (FC S) (Gibco) and 1% L-Glutamine/Penicillin/Streptomycin (Biological Industries). 12-hours post IT-injection, the mice were administered with another dose of carprofen (5 mg/kg). The mice were monitored for about one-four months for tumor development.

To validate the inhibitory effect of simvastatin (SVA) *in vivo*, NOD/SCID mice that developed OS tumors after IT injection were split randomly into two groups, mice that received 60 mg/kg/day SVA (8-mice), and a vehicle group (6-mice). The two groups received a gavage injection for 10 days, then the mice were euthanized, and tumors were collected for further analysis.

Ethical Compliance: All procedures performed in studies involving animal use were in accordance with the ethical standards of the institutional and/or national research committee.

Bone Marrow (BM) extraction and culture:

BM cells were collected from WT mice (control), young non-tumor-bearing SKO and DKO-Osx1-Cre-tdTomato mice at different time points (yBM), as well as at the time of tumor detection (BMT). Mice were sacrificed using CO_2, femurs and tibiae from both legs were cleaned from connective tissue, and the BM was flushed out using a syringe with 27 Gauge needle. Red blood cells were lysed using a hypotonic treatment (water dilution). The cells were then centrifuged, filtered, and plated at an appropriate density after one passage (p1).

Tumor dissection and tumor cell lines preparation:

At the time of tumor detection, mice were euthanized, and tumors were extracted and minced using a sterile scalpel and digested with trypsin (25 mg/ml), Collagenase P (1 mg/ml), and DNase (10 mg/ml) for 1hour at 37 ^{o}C with vigorous shaking. Cells were then filtered through 70µM filter, centrifuged, and plated in 10 cm^2 plates in 10% MEM-α medium.

Flow Cytometry analysis of the mesenchymal and hematopoietic markers

$1x10^6$ of yBM, BMT, and tumor cells were collected freshly (direct) and/or after culture (Cult)- when the tdTomato positive cells were dominant. Cells were stained with FACS buffer (2% FCS, 1mM EDTA, 0.1% Sodium Azide in PBS), containing the following antibodies: for mesenchymal markers, Sca-1 (D7, Biolegend,1:250), CD29 (HMβ1-1, BioLegend, 1:250), and for hematopoietic markers; CD45.2 (104, BioLegend, 1:100), for 30 min at 4 ^{o}C. Samples were acquired using a CytoFlex cytometer and analyzed using CytExpert version 2.4.

Osteogenic Differentiation of yBM, BMT and tumor cells

yBM, BMT, and tumor cells were induced to differentiate by plating them at 70% confluency, and culturing in osteogenic medium that included 10% MEMα supplemented with Ascorbic Acid (50µg/ml) and β-glycerophosphate (3mM). Osteogenic medium was added and replaced every 2-3 days for 21 days. Mineralization was assessed by measuring the expression levels of osteogenic markers (real-time PCR-as explained later in real time PCR section), and the formation of calcium-enriched nodules was detected by Alizarin Red Staining.

Colony formation assay:

Five hundred yBM, BMT, and tumor cells were seeded in 6-well plates (triplicate), and the colonies were monitored for one week. The colonies were then fixed using absolute methanol for 10 min and stained with Gimza stain for 30 min. The colonies were then washed and counted. The graph shows fold change/number of colonies compared to the control groups, and bars represent standard deviation (SD).

To determine the effect of simvastatin (SVA) on the survival of yBM, BMT, and tumor cells, 24 h after seeding, SVA was added at the indicated concentrations for 48 h, and colonies were monitored for one week. Fixation, staining, and analysis were performed as previously described.

Wound Healing- Scratch Assay-Migration

The migration abilities of yBM, BMT, and tumor cells were determined using a wound healing scratch assay. $3x10^4$ yBM, BMT, and tumor cells were seeded in a 96-well ImageLock™ tissue culture plate for 12 h. Then, a scratch was made using the WoundMaker ™, and the wells were washed three times with culture media, followed by the addition of serum-free media (SFM). The plates were incubated in IncuCyte ZOOM and schedule repeat scanning was performed every 2 h for 72 h.

Wound Healing- Scratch Assay-Invasion

The invasive abilities of yBM, BMT, and tumor cells were determined using a wound healing scratch assay. A 96-well ImageLock™ tissue culture plate was coated with matrigel for 12 h. Next, $3x10^4$ yBM, BMT, and tumor cells were seeded for 12 h. A scratch was made using the WoundMaker ™, followed by washing three times with culture media, then 100µl of media was added. The plate was cooled to 4 °C for 5 min, the media was removed, a top layer of Matrigel (50µl) was added, and the plate was incubated at 37 °C for 30 min, before adding another 100µl. The plates were incubated in IncuCyte ZOOM and schedule repeat scanning was performed every 2 h for 72h.

Cell Proliferation assay (MTT assay):

To check the effect of SVA on cell viability, yBM, BMT, and tumor cells ($3x10^3$) were seeded in 96 well plate (triplicate for each group and for each concentration), at 24-hours intervals. Then, activated SVA (as explained later) was added at the indicated concentrations for 48 h and analyzed using the MTT reagent according to the manufacturer's instructions. The graph represents the comparison with the control group, and the bars represent ± the SD.

For SVA activation, 4 mg of simvastatin was dissolved in 100µl of ethanol. Then 150µl of 0.1NaOH was add to the solution and incubated at 50 °C for 2 h. The pH was brought to 7.0, and the final concentration of the stock solution was 4 mg/ml. The stock solution was stored at 4 °C.

Immunoblotting:

Total protein was lysed by using lysis buffer containing 50 mM Tris (pH7.5), 150 mM NaCl, 10% glycerol, 0.5% Nonidet P-40 (NP-40), with addition of protease and phosphatase inhibitors (1:100). The lysates were subjected to SDS-PAGE under

standard conditions. The following antibodies were used: rabbit polyclonal WWOX 1:10000, mouse monoclonal Gapdh (CB-1001-), Calbiochem 1:10000, mouse monoclonal p21(F-5), sc 6246, Santa Cruz 1:200, mouse monoclonal p53 (1C12), Cell Signaling, 1:1000, mouse monoclonal MCM7 (141.2), sc-9966- Santa Cruz 1:200, rabbit polyclonal c-Myc (9402)-Cell Signaling, 1:750, rabbit polyclonal DsRed (632496), TaKaRa, 1:500, and mouse monoclonal β-actin (A5441), Sigma 1:10000.

Histology and Immunohistochemistry

Fixed bones and tumors [4% formalin] were partially decalcified in 14% EDTA for three days, followed by paraffin embedding, sectioning then staining with hematoxylin and eosin (H&E). For Immunohistochemistry, paraffin-embedded tissues were deparaffinized, followed by antigen retrieval with 25mM citrate buffer (PH 6) in a pressure cooker. Then, the sections were left to cool for 25 min, followed by blocking of the endogenous peroxidase with 3% H_2O_2 for 15 min. To reduce non-specific binding of the primary antibody, tissues were blocked with blocking solution (CAS Block), followed by incubation with the primary antibody overnight at 4°C. Sections were washed with TBST, followed by incubation with secondary anti-rabbit or anti-mouse immunoglobulin antibody for 30 min. The reaction was then performed using a DAB peroxidase kit (Vector Laboratories, SK-4100), followed by hematoxylin staining for 40s as a counterstain. IHC stains were manually counted, at least five pictures were taken for each slide, and the average was calculated for each slide. The antibodies used were mouse monoclonal MCM7 (141.2) [sc-9966- Santa Cruz 1:200].

Immunofluorescence

Bones (Femur and Tibia) were fixed in 4% PFA overnight at 4 °C. Fixed bones were partially decalcified in 14% EDTA for 3 days, washed in a sucrose gradient (1 h in 10% sucrose, 1 h in 20% sucrose, overnight in 30% sucrose) before snap-freezing them in OCT embedding medium. Frozen sections were cut at 10μm

thickness and stored at -80 °C. Sections were warmed to room temperature, washed in PBS, fixed with 4% PFA for 10 minutes then washed two times with PBS. The sections were incubated with Hoechst 33258 diluted in 5% normal goat serum, 0.05% BSA and 0.1 %Triton X-100 in PBS for 15-minutes. The slides were then dried and mounted with coverslips using immunofluorescence mounting medium (Dako s3023). Sections were then imaged using an Olympus FLUO-VIEW FV1000 confocal laser scanning microscope and processed using the associated Olympus FLUO VIEW software.

For paraffin-embedded sections, after deparaffinization and antigen retrieval, as mentioned above, tissues were blocked using a blocking solution (5% normal goat serum, 0.05% BSA, and 0.1 %Triton X-100 in PBS) for 40-minutes. The sections were then incubated with the primary antibody diluted in the blocking solution overnight at 4ºC °C. The following day, the sections were washed 3-times with PBSx1, incubated with secondary antibody and Hoechst 33258 diluted in blocking solution for 1-hour at room temperature, then washed 3-times with PBSx1. The slides were then dried, mounted, and imaged as described above. The antibody used was rabbit polyclonal DsRed (632496; TaKaRa, 1:500).

Real Time PCR:

Total RNA was extracted using TRI reagent (Biolab), as described by the manufacturer for the phenol/chloroform-based method. cDAN was prepared with 1µg of RNA using a QScript cDNA synthesis kit (Quantabio). The SYBR Green PCR Master Mix (Applied Biosystems) was used for qRT-PCR. All measurements were performed in triplicate and standardized to HPRT levels. The primer sequences are listed in Table 1.

RNA Sequencing and analysis:

Four WT, six non-tumor bearing, and six tumor-bearing mice were euthanized by CO_2, and BM and/or tumor were extracted and cultured as described above. After three passages, tdTomato-positive cells were dominant in the culture, and RNA was prepared using the TRI reagent (Biolab). Library preparation and sequencing were performed by the Genomic Applications Laboratory in Hebrew University's Core Research Facility using a standard protocol. RNA quality was checked using a tape station (Agilent Technologies), followed by poly-A cleanup and cDNA preparation. To prepare cDNA, 1 µg of RNA from each sample was processed using the KAPA Stranded mRNA-Seq Kit with mRNA Capture Beads (Kapa Biosystems). Sequencing was performed using NextSeq 500 (Illumina). For library quality control, measures were applied to raw FASTQ files, trimming low-quality bases (Q>20), residual adapters, and filtering out short reads (L>20). These measurements were performed with the Trim-Galore (v0.4.1) wrapper tool. File assessment before and after quality control was performed using FastQC (v0.11.5). The mouse transcriptome was mapped using salmon v0.13.1. Differential gene expression for the 16 samples was explored using the R package (v1.16.1) and analyzed using DESeq2 (v1.28.1).

Data Access Statement: Raw data are available upon reasonable request.

Statistical analysis:

The results of the experiments are expressed as mean± SD. The Student's t-test was used to compare the values of the test and control samples. p-value ≤ 0.05 indicates a significant difference; ** $p \leq 0.01$, *** $p \leq 0.001$, **** $p \leq 0.0001$.

Results:

Generation of a traceable mouse model of osteosarcoma

We have recently shown that depletion of both *Wwox* and *p53* (DKO) in osteoblast progenitors, using *Osterix1-Cre*, accelerates osteosarcoma (OS) development, resulting in more aggressive and chemotherapy-resistant OS than *p53* knockout alone (SKO)[11]. To better dissect the early molecular events contributing to osteosarcomagenesis, we bred our DKO mouse model with *Rosa26-LSL-tdTomato* transgenic mice (Figure 1A). Depletion of *Wwox* and *p53* and the expression of *tdTomato* (DKO^{TOM}) were confirmed by genomic PCR (Figure 1B). Expression of the tdTomato reporter in osterix-expressing cells was validated by fluorescence microscopy (Figure 1C). Consistent with previous work[23], tdTomato-positive cells expressing *Osterix* were also detected in the bone marrow (BM) of young non-tumor-bearing mice, as validated by immunofluorescence of bone-frozen sections (Figure 1D) and flow cytometry analysis of BM cells (Figure1E). Ablation of WWOX and p53 in cultured tdTomato-positive BM cells was also confirmed at the protein level after exposure to ionizing radiation by immunoblot analysis (Figure 1F). In agreement with our previous findings, DKO^{TOM} mice developed OS with a latency of 8-months (data not shown), as previously shown for DKO[11]. Using this new mouse model, we next determined the molecular and cellular changes that occur during OS development.

Bone marrow cells of OS-bearing mice are tumorigenic

To elucidate the kinetics of OS tumor formation in DKO^{TOM} mice, we examined the presence of tomato florescence in different compartments. Interestingly, we detected a high percentage of tdTomato-positive cells both in the directly collected tumor (Direct-Tumor) and BM of DKO^{TOM} tumor-bearing mice (Direct-BMT) (Figure 2A). These results prompted us to test whether BMT cells exhibit tumorigenic abilities. To this end, we isolated and cultured tdTomato BMT and tumor cells and examined their ability to survive and proliferate *in vitro*. We found that BMT cells

were able to form colonies similar to those isolated from the DKO^{TOM} tumor itself (Figure 2B), as compared to BM cells isolated from wild-type mice (Cre+WT;tomato), which failed to form any colonies, as expected. We next examined the tumorigenic capability of BMT cells *in vivo* and found that 78% of the immunocompromised mice that were intratibially (IT) injected with BMT cells were able to develop tomato-positive osteoblastic OS, as validated by H&E and immunofluorescence staining, respectively (Figure 2C). As expected, mice injected with wild-type BM cells (control) did not form any tumors. Notably, it took more time for BMT cells to develop tumors as compared to the paired primary tumor cells, suggesting that other hits are earned in the tumor itself (Figure 2D). More interestingly, these BMT cells exhibited prometastatic properties, as assessed by wound healing ability *in vitro*, both migration and invasion (Figure 2E, F).

Next, we sought to characterize the identity of the BMT cells. Immunophenotyping of the isolated BMT cells [direct] revealed a high percentage of CD45 hematopoietic cells (consistent with a recent study confirming the expression of osterix in the hematopoietic lineage)[25] surface markers and the presence of a minor population of mesenchymal origin, expressing cell surface markers of CD29 and Sca-1 (Figure 1S-A, Bi). Similar results were obtained for the tumor cells (Figure 1S-A, Bii). However, culturing of BMT and tumor cells [culture] led to the expansion of the mesenchymal population that was tdTomato-positive and diminished the hematopoietic population (Figure 1S-A, Bi-Bii). Importantly, these cultured BMT- and tumor-tdTomato-positive cells expressed high levels of osteogenic markers, indicating their osteoblast identity (Figure 1S-C). In addition, BMT cells were able to differentiate toward the osteoblastic lineage, as validated by Alizarin red staining and mRNA levels of osteoblast markers, although less efficiently than tumor cells. (Figure 1S-D, E).

After demonstrating the tumorigenic ability of BMT cells, we investigated the molecular characteristics contributing to OS development. Therefore, we performed RNA sequencing analysis on the cultured control BM, BMT, and primary

OS tumor cells of DKO mice. Using principal component analysis (PCA), we found that BMT and tumor cells clustered together in PC2 away from the control BM cells (Figure 3A). Strikingly, these BMT cells had 164 mutual deferential expressed (DE) genes in the tumor cells, as shown in the Venn diagram analysis (Figure 3B). Using unsupervised clustering analysis, we found that many OS-known genes were differentially upregulated (Rrp9, Rcc1, Ran), while others were downregulated (Mylk, Nid2) in the BMT and tumor cells compared to the control BM cells (Figure 3C). Pathway enrichment analysis and gene set enrichment analysis (GSEA) revealed significant changes in genes associated with the cell cycle (E2F and Myc targets) and DNA repair pathways (Figure 3D, E). Taken together, these data suggest that BMT cells isolated from OS-bearing mice are tumorigenic and, to a large extent, mirror OS tumor cells.

young BM (yBM) cells exhibit tumorigenic ability

Our data imply that the BMT cells of DKO mice have tumorigenic abilities. Hence, we hypothesized that they might be used as proxies to dissect early molecular events contributing to osteosarcomagenesis. To address this, we collected BM cells from young non-tumor bearing mice (yBM) of different ages (1.5-6 months) of DKO mice and examined their cellular and molecular features. Intriguingly, we found that there was an increase in the percentage of tdTomato-positive cells in both wild type and genetically manipulated (DKO) yBM cells, which expanded with time in the latter (Figure 4A).

We next validated that the yBM cells were of mesenchymal origin (Figure 2S- A, B), as observed previously for BMT cells. In addition, these yBM cells exhibited increased levels of osteogenic markers (Figure 2S-C) and differentiation capability, as assessed by Alizarin Red staining and qPCR analysis (F1S-D, E,). Remarkably, yBM cells isolated from DKO mice were able to form colonies (Figure 4B) and generate OS tumors upon IT injection in immunocompromised mice (Figure 4C). The latency of forming OS tumors was 3-months with penetrance that ranged from 36%-50% (Figure 4D). Histological analysis of these tomato-positive tumors

revealed both fibroblastic and osteoblastic characteristics (Figure 4C). Altogether, these findings support our initial assumption that the BM cells in our DKO OS model can be used as a surrogate to investigate osteosarcomagenesis.

As the main hurdle in OS is the detection of lung metastasis at diagnosis, we tested whether these DKO yBM cells from non-tumor-bearing mice could exhibit migration and invasion abilities. Remarkably, DKO yBM cells, as well as BMT and tumor cells, demonstrated migration and invasion abilities, as validated by a wound healing assay *in vitro* (Figure 2S D, E). To further validate migration and invasion abilities *in vivo*, we intravenously injected yBM cells into NOD/SCD mice. Surprisingly, these cells were able to colonize the lungs and form nodules, as validated by immunofluorescence and H&E staining (Figure 4E), as indicated in the bar graph (Figure 4F) Taken together, these data suggest that DKO yBM cells isolated from non-OS-bearing mice display tumorigenic traits that could potentially reflect changes in OS tumor cells.

Early molecular changes contributing to osteosarcomagenesis

Our previous results have demonstrated the tumorigenic ability of yBM cells isolated from non-OS-bearing mice. Next, we investigated the molecular characteristics of yBM DKO cells that contribute to OS development. Therefore, we performed RNA sequencing analysis on control BM, yBM, and primary OS tumor cells of DKO mice. Using PCA, we found that the DKO yBM and tumor cells clustered together away from the control BM cells (Figure 5A). Strikingly, these yBM cells had 303 mutual genes with the tumor cells, as shown in the Venn diagram (Figure 5B). In addition, when we compared the DE genes between DKO yBM and BMT cells, they clustered together away from the control BM cells (Figure 5D). As shown in Figure 5E, 471 genes were common between yBM and BMT cells. Using unsupervised clustering analysis, we found that the upregulated and downregulated DE genes in the yBM and tumor cells, and in the yBM and BMT cells clustered together away from the control BM cells (Figure 3S-A, B). Pathway enrichment analysis and GSEA between yBM and tumor cells and between yBM

and BMT cells revealed significant changes in genes associated with the cell cycle (E2F targets, c-Myc targets, and G_1S transition) and DNA repair pathways (Figure 5C, F, G, H), consistent with those observed between BMT and tumor cells (Figure 3).

Altogether, these data imply that there is a high similarity between DKO yBM, BMT, and OS tumor genetic makeup, making yBM cells of DKO mice a possible surrogate for studying OS.

***Trp53* SKO yBM is not tumorigenic.**

To test whether the observed changes were unique to DKO tumors or common to other mouse models, we generated a traceable mouse model harboring a*Trp53* KO alone and expressing tdTomato (SKO^{TOM}) under the control of the same Osx1-Cre model (Figure 4S-A). SKO^{TOM} was validated using genomic PCR (Figure 4S-B). Importantly, SKO^{TOM} mice developed OS tumors at a median age of 11 months (data not shown), as previously shown[11].

We next validated the expression of our genetic manipulation in the BM cells of SKO^{TOM} mice (Figure 4S-C). Consistent with the DKO model, we observed an age-dependent increase in the percentage of tomato-positive cells (Figure 4S-D). In addition, we found that these tomato-positive BM cells were of mesenchymal origin (Figure 4S-E and F), similar to those observed in DKO^{TOM} mice.

Next, we injected SKO yBM cells into NOD/SCID mice. None of the mice injected with SKO yBM cells formed tumors, even after 3-4 months of injection (Figure 5S-A, B). Interestingly, when we subjected SKO yBM cells to RNA sequencing, we found low expression of Myc and its targets. Indeed, when we compared the transcriptomics of DKO yBM cells to SKO yBM cells, we observed that the Myc target pathway was unique to yBM-DKO cells (Figure 6A, B). Both RNA sequencing and qPCR data analysis indicated enhanced upregulation of Myc targets in DKO cells relative to that in SKO yBM cells (Figure 6C, D). Further comparisons of SKO yBM with DKO tumor and BMT cells (Figure 3S-C, D)

indicated that Myc targets are unique to DKO tumors and BMT cells. Moreover, a comparison of SKO yBM cells and SKO tumor cells showed that Myc targets were unique to SKO tumor cells (Figure 3S-E). Surprisingly, Myc targets were mutually expressed between SKO and DKO tumors (Figure 3S-F), suggesting that the Myc pathway is indispensable at the tumor stage. These data indicate that Myc targets are the prominent pathway contributing to earlier stages of osteosarcomagenesis.

MCM7 upregulation in DKO yBM cells contributes to their tumorigenic ability

Molecular analysis revealed that the Myc pathway was one of the most prominent and significant early events in DKO yBM cells. This is consistent with previous studies demonstrating the upregulation of Myc in human OS[26,27]. Intriguingly, RNA sequencing analysis also showed the upregulation of Myc targets (Figure 3S-G, H), including MCM7, related to cell cycle regulation and DNA replication[14]. MCM7 upregulation was validated at the mRNA (Figure 7A) and protein levels as assessed by western blotting (Figure 7B-upper panel). We further detected a higher level of Myc and Myc target-MCM7 in DKO yBM cells than that in SKO yBM cells (Figure 5S-C), which likely explains the higher survival ability of DKO yBM cells, as validated by the higher number of colonies (Figure 5S-D).

Targeting MCM7 by statins has recently been shown to have an inhibitory effect on the proliferation of tumor cells [18]. We next examined the effect of MCM7 inhibition on the proliferation of DKO yBM, BMT, and mouse OS tumor cells. We found that increased doses of simvastatin (SVA), previously shown to inhibit MCM7[18], inhibited the growth of yBM cells similar to that of OS tumor cells and BMT, but did not affect control BM cells (Figure 7C). In addition, we observed a dose-dependent inhibitory effect on the survival of DKO yBM, BMT, and tumor cells (Figure 7D). This treatment was accompanied by decreased MCM7 and Myc protein levels (Figure 7B-lower panel), consistent with a previous work[19]. Moreover, the DKO yBM was more sensitive to SVA than the SKO yBM (Figure 7E).

Next, we examined the inhibitory effect of SVA on tumor growth *in vivo*. After tumor detection due to IT injection of DKO yBM and tumor cells in immunocompromised NOD/SCID mice, the mice were treated with vehicle or SVA (60 mg/kg/day) via gavage for an additional 10-days. We observed a significant decrease in the tumor size and weight following SVA treatment (Figure 7F). Interestingly, we also noticed a significant reduction in MCM7 levels in SVA-treated tumors, as validated by IHC (Figure 7G). Collectively, these data imply that MCM7, a Myc target gene, plays an important role in the early stages of osteosarcomagenesis.

Discussion:

High genetic heterogeneity and chromosomal instability contributes to worse prognosis in OS[3]. Hence, understanding the early molecular events in osteosarcomagenesis is crucial and could provide insights into early biomarkers and aid in the development of alternative therapies. In the present study, using the *Osterix1-cre* transgenic mouse model, we showed that deletion of *Wwox* and *Trp53* (DKO), while expressing the tdTomato reporter, resulted in the presence of genetically manipulated osterix-expressing cells in the BM. Interestingly, these genetically manipulated cells collected at the time of tumor detection expressed mesenchymal and osteoblastic markers, similar to OS tumor cells. In addition, BM cells isolated from DKO non-OS-bearing mice exhibited tumorigenic traits, as well as cellular and molecular changes resembling those of OS tumor cells and paired BM cells from OS-bearing mice. Our traceable OS mouse model facilitated examination and validation of molecular changes that occur during the early stages of osteosarcomagenesis. We found that Myc and its target genes were key players in the early stages of OS development. Inhibition of these targets may hamper the development of OS.

The cell of origin for OS remains controversial, with some studies suggesting that MSCs are the cell of origin[28]. p53 has been extensively shown to play a central role in OS development in both human and mouse models[29,22]. Interestingly, p53

knockdown alone is not enough to transform human MSCs (hMSCs) to induce osteosarcomagenesis[28], which may indicate that at this stage, there is a need for additional hits to trigger the initiation of osteosarcoma. Consistent with these results, our data demonstrate that murine yBM cells collected from mice harboring the deletion of *Trp53* alone (SKO) were not tumorigenic, whereas yBM cells collected from DKO mice harboring the deletion of both *Wwox* and *Trp53* exhibited tumorigenic traits and closely resembled OS tumor cells. These findings indicate that loss of WWOX at earlier stages of tumorigenesis promotes osteosarcomagenesis. Our observation is in agreement with a previous study[28] that demonstrated that human MSCs transformed by Rb knockdown and c-Myc overexpression resulted in OS development and that these cells lost their mesenchymal stem cell markers and became more committed to the osteoblast lineage[28]. Interestingly, we detected both mesenchymal and osteoblast markers in BM-MSCs using our yBM model. This may indicate that the specific genetic manipulation of the combined loss of WWOX and p53 under the *Osterix* promoter in our model could provide cells with plasticity to express both mesenchymal and osteoblast markers, thus transdifferentiating and contributing to the formation of a histological spectrum of OS.

OS is generally associated with alterations in the expression of genes involved in cell cycle regulation and apoptosis[30]. Myc also plays an important role in the development and progression of OS. Notably, more than 10% of OS patients have c-Myc amplification[26,27] and many more exhibit overexpression of Myc[31,13,32]. Interestingly, our yBM collected from a tumor-free mouse and BMT cells share several genes with OS tumors. These genes are related to cell cycle pathways, DNA repair and c-Myc targets. Detecting high levels of Myc in OS tumors is consistent with previous studies[31,13,32], however its expression in yBM of DKO cells further strengthen that these cells resemble OS tumors and their indispensable role in osteosarcomagenesis.

Remarkably, our DKO yBM cells expressed high levels of c-Myc in comparison to SKO-yBM cells, and this differential expression of c-Myc and its target genes

resulted in cellular advantage to DKO yBM, both *in vitro* and *in vivo*. Although c-Myc upregulation has been shown in p53-deficent OS tumors[33], our study provide clear evidence that combined deletion of WWOX and p53 resulted in increased Myc levels and activity in BM-MSCs as well as formation of indistinguishable OS tumors. This combined genetic manipulation seems to be critical for OS initiation since p53-decicient BM-MSCs, at the same stage, didn't result in tumor formation *in vivo* further implying the significance of WWOX deletion in initiation of p53-deficiecnt OS tumors.

Given that c-Myc upregulation has been shown to cooperate with other tumor suppressor genes to transform hMSCs to form OS[28] we assumed that our model recapitulates human OS and that the combined deletion of WWOX and p53 is critical for the initiation of OS. Importantly, we propose that yBM cells can be used as surrogates to investigate the early stages of osteosarcomagenesis. Moreover, our study validate that the BM-MSCs with co-deletion of WWOX and p53 are tumorigenic compared to p53 deletion alone although with a later latency as compared with BM-MSCs harboring p53 and Rb co-deletion[34]. Furthermore, our DKO yBM model exhibited early molecular pathway enrichment, which is consistent with a recent multi-omics analysis performed on human OS clinical samples[35]. Interestingly, Myc amplification and overexpression of Myc targets were detected and correlated with a worse prognosis, indicating the crucial role of Myc in osteosarcomagenesis. Moreover, this analysis of human OS clinical samples further indicated the alteration of several tumor suppressor genes, including *TP53* and *WWOX* deletion, which further strengthens our model recapitulates human OS. In addition, it also showed that deletion of *RB1*, resulting in the attenuation of cell cycle-related pathways, which is also one of the most prominently altered pathways in our model. Moreover, single-cell RNA sequencing performed in human OS samples and the construction of a novel OS classification model revealed three subtypes of OS that exhibit distinct prognoses and different expression levels of therapy-related genes[36], where some of these genes are differentially expressed in murine DKO-yBM cells, such as Myc and CDK4.

In addition to the role of c-Myc itself, we validated c-Myc activity by examining one of the c-Myc targets, MCM7. MCM7 is part of the MCM complex, plays an important role in cell cycle initiation, and is upregulated in several tumors, including sarcomas[15,16]. Interestingly, DKO yBM showed upregulation of MCM7 in an age-dependent manner at both mRNA and protein levels. High levels of MCM7 protect the cell by acting as a guardian and inducing genomic stability, thus making the cells more resistant to replication stress caused by chemotherapy[18]. As MCM complex components are present in excess in the cells and act as a dormant origin, once these excess amounts are depleted, the cells will be more sensitive to replicative stress[17], making them a good therapeutic target.

Statins are competitive inhibitors of 3-hydroxy-3-methylglutaryl-coenzyme A (HMG-CoA) reductase, a rate-limiting enzyme that converts HMG-CoA to mevalonate during cholesterol synthesis [37]. In addition to their traditional role in lowering serum cholesterol levels, extensive studies have suggested that statins inhibit carcinogenesis[38,39,40] and can be used in cancer therapy[41,42]. Furthermore, studies suggested that statin administration prior to cancer diagnosis exhibited reduced cancer related mortality by up to 15%[43] and showed that long term use of statins reduces the risk of colorectal cancer[44].

Interestingly, MCM7 can be targeted by statins, generating more DNA damage and inhibiting cell proliferation[18,19]. Our data demonstrated that MCM7 inhibition by SVA reduced cell proliferation and survival in a dose-dependent manner. Importantly, DKO yBM, but not SKO yBM, survived better and exhibited a higher sensitivity. The significant inhibitory effect of SVA can be attributed to the central role of MCM7 in cell fate. It is also possible that SVA has effects that go beyond inhibition of MCM7. In addition, SVA treatment *in vivo* resulted in a reduction in tumor size and weight, which was accompanied by a decrease in MCM7 protein levels.

Conclusions

Consistent with their roles as tumor suppressor genes, the combined deletion of WWOX and p53 in Osx1-positive progenitor cells resulted in their transformation and growth advantage. This advantage is mediated by c-Myc overexpression during early stages of OS cell proliferation and survival. Given that p53 alone is not sufficient to drive the early molecular changes observed, WWOX silencing and c-Myc overexpression may be considered targets for the prevention and treatment of OS patients. Further studies are needed to explore the underlying mechanism of how WWOX and p53 loss mediate upregulation of c-Myc to transform MSCs into OS-like cells. Our study provides a cellular and genetic platform to study the mechanisms underlying OS transformation, progression, and treatment.

Acknowledgments

We are grateful to Dr. Sri Repudi, Ms. Natalie Kaufman and Ms. Randa Tissawak for their help and technical assistance, and to Mr. Jonathon Monin for bioinformatic analysis. The Aqeilan's lab is funded by the European Research Council (ERC) [No. 682118] to R.I.A and the Bi-national Science Foundation (BSF) [No. 2017269] to R.I.A and G.S.S.

References:

1. Mirabello, L., Troisi, R. J. & Savage, S. A. Osteosarcoma incidence and survival rates from 1973 to 2004: data from the Surveillance, Epidemiology, and End Results Program. *Cancer* **115**, 1531–1543 (2009).

2. Casali, P. G. *et al.* Bone sarcomas: ESMO Clinical Practice Guidelines for diagnosis, treatment and follow-up. *Ann. Oncol. Off. J. Eur. Soc. Med. Oncol.* **25 Suppl 3**, iii113–iii123 (2014).

3. Gok Durnali, A. *et al.* Outcomes of Adolescent and Adult Patients with Lung Metastatic Osteosarcoma and Comparison of Synchronous and Metachronous Lung Metastatic Groups. *PLoS One* **11**, e0152621 (2016).

4. Gill, J., Ahluwalia, M. K., Geller, D. & Gorlick, R. New targets and approaches in osteosarcoma. *Pharmacol. Ther.* **137**, 89–99 (2013).

5. Gorlick, R. & Khanna, C. Osteosarcoma. *J. Bone Miner. Res.* **25**, 683–691 (2010).

6. Mutsaers, A. J. & Walkley, C. R. Cells of origin in osteosarcoma: mesenchymal stem cells or osteoblast committed cells? *Bone* **62**, 56–63 (2014).

7. Del Mare, S., Salah, Z. & Aqeilan, R. I. WWOX: Its genomics, partners, and functions. *J. Cell. Biochem.* **108**, 737–745 (2009).

8. Aqeilan, R. I. & Croce, C. M. WWOX in biological control and tumorigenesis. *J. Cell. Physiol.* **212**, 307–310 (2007).

9. Salah, Z., Aqeilan, R. & Huebner, K. WWOX gene and gene product: tumor suppression through specific protein interactions. *Future Oncol.* **6**, 249–259 (2010).

10. Kurek, K. C. *et al.* Frequent attenuation of the WWOX tumor suppressor in osteosarcoma is associated with increased tumorigenicity and aberrant RUNX2 expression. *Cancer Res.* **70**, 5577–5586 (2010).

11. Del Mare, S. *et al.* WWOX and p53 Dysregulation Synergize to Drive the Development of Osteosarcoma. *Cancer Res.* **76**, 6107–6117 (2016).

12. Kansara, M., Teng, M. W., Smyth, M. J. & Thomas, D. M. Translational biology of osteosarcoma. *Nat. Rev. Cancer* **14**, 722–735 (2014).

13. Gamberi, G. *et al.* C-myc and c-fos in human osteosarcoma: prognostic value of mRNA and protein expression. *Oncology* **55**, 556–563 (1998).

14. Yu, S. *et al.* MCMs in Cancer: Prognostic Potential and Mechanisms. *Anal. Cell. Pathol. (Amst).* **2020**, (2020).

15. Toyokawa, G. *et al.* Minichromosome Maintenance Protein 7 is a potential therapeutic target in human cancer and a novel prognostic marker of non-small cell lung cancer. *Mol. Cancer* **10**, (2011).

16. Zhou, J. *et al.* Expression and Prognostic Value of MCM Family Genes in Osteosarcoma. *Front. Mol. Biosci.* **8**, 601 (2021).

17. Ibarra, A., Schwob, E. & Méndez, J. Excess MCM proteins protect human cells from replicative stress by licensing backup origins of replication. *Proc. Natl. Acad. Sci. U. S. A.* **105**, 8956–8961 (2008).

18. Li, J. *et al.* Simvastatin and Atorvastatin inhibit DNA replication licensing factor MCM7 and effectively suppress RB-deficient tumors growth. *Cell Death Dis.* **8**, e2673 (2017).

19. Liang, Z. *et al.* Simvastatin suppresses the DNA replication licensing factor MCM7 and inhibits the growth of tamoxifen-resistant breast cancer cells. *Sci. Rep.* **7**, (2017).

20. Yang, Y. *et al.* Genetically transforming human osteoblasts to sarcoma: development of an osteosarcoma model. *Genes Cancer* **8**, 484–494 (2017).

21. Rubio, R. *et al.* The differentiation stage of p53-Rb-deficient bone marrow mesenchymal stem cells imposes the phenotype of in vivo sarcoma

development. *Oncogene* **32**, 4970–4980 (2013).

22. Walkley, C. R. *et al.* Conditional mouse osteosarcoma, dependent on p53 loss and potentiated by loss of Rb, mimics the human disease. *Genes Dev.* **22**, 1662 (2008).

23. Chen, J. *et al.* Osx-Cre Targets Multiple Cell Types besides Osteoblast Lineage in Postnatal Mice. *PLoS One* **9**, e85161 (2014).

24. S, D. M. *et al.* WWOX and p53 Dysregulation Synergize to Drive the Development of Osteosarcoma. *Cancer Res.* **76**, 6107–6117 (2016).

25. Ricci, B. *et al.* Osterix-cre marks distinct subsets of CD45-and CD45+ stromal populations in extra-skeletal tumors with pro-tumorigenic characteristics. *Elife* **9**, 1–29 (2020).

26. Martin, J. W., Squire, J. A. & Zielenska, M. The genetics of osteosarcoma. *Sarcoma* **2012**, (2012).

27. Smida, J. *et al.* Genomic alterations and allelic imbalances are strong prognostic predictors in osteosarcoma. *Clin. Cancer Res.* **16**, 4256–4267 (2010).

28. Wang, J.-Y. *et al.* Generation of Osteosarcomas from a Combination of Rb Silencing and c-Myc Overexpression in Human Mesenchymal Stem Cells. *Stem Cells Transl. Med.* **6**, 512–526 (2017).

29. Chen, X. *et al.* Recurrent somatic structural variations contribute to tumorigenesis in pediatric osteosarcoma. *Cell Rep.* **7**, 104–112 (2014).

30. Kleinerman, E. S. & Rao-Bindal, K. Epigenetic regulation of apoptosis and cell cycle in osteosarcoma. *Sarcoma* **2011**, (2011).

31. Feng, W. *et al.* Myc is a prognostic biomarker and potential therapeutic target in osteosarcoma. *Ther. Adv. Med. Oncol.* **12**, (2020).

32. Jain, M. *et al.* Sustained loss of a neoplastic phenotype by brief inactivation of MYC. *Science (80-.).* **297**, 102–104 (2002).

33. Otani, S. *et al.* Runx3 is required for oncogenic Myc upregulation in p53-deficient osteosarcoma. *Oncogene* **41**, 683–691 (2022).

34. Berman, S. D. *et al.* Metastatic osteosarcoma induced by inactivation of Rb and p53 in the osteoblast lineage. *Proc. Natl. Acad. Sci. U. S. A.* **105**, 11851–11856 (2008).

35. Jiang, Y. *et al.* Multi-omics analysis identifies osteosarcoma subtypes with distinct prognosis indicating stratified treatment. *Nat. Commun.* **13**, 1–17 (2022).

36. Zhang, H. *et al.* A novel molecular classification method for osteosarcoma based on tumor cell differentiation trajectories. *Bone Res.* **11**, (2023).

37. Goldstein, J. L. & Brown, M. S. Regulation of the mevalonate pathway. *Nature* **343**, 425–430 (1990).

38. Glynn, S. A., O'Sullivan, D., Eustace, A. J., Clynes, M. & O'Donovan, N. The 3-hydroxy-3-methylglutaryl-coenzyme A reductase inhibitors, simvastatin, lovastatin and mevastatin inhibit proliferation and invasion of melanoma cells. *BMC Cancer* **8**, (2008).

39. Gopalan, A., Yu, W., Sanders, B. G. & Kline, K. Simvastatin inhibition of mevalonate pathway induces apoptosis in human breast cancer cells via activation of JNK/CHOP/DR5 signaling pathway. *Cancer Lett.* **329**, 9–16 (2013).

40. Von Tresckow, B. *et al.* Simvastatin-dependent apoptosis in Hodgkin's lymphoma cells and growth impairment of human Hodgkin's tumors in vivo. *Haematologica* **92**, 682–685 (2007).

41. Brower, V. Of Cancer and Cholesterol: Studies Elucidate Anticancer Mechanisms of Statins. *JNCI J. Natl. Cancer Inst.* **95**, 844–846 (2003).

42. The statins as anticancer agents - PubMed. https://pubmed.ncbi.nlm.nih.gov/12538446/.

43. Nielsen, S. F., Nordestgaard, B. G. & Bojesen, S. E. Statin Use and Reduced Cancer-Related Mortality. *N. Engl. J. Med.* **367**, 1792–1802 (2012).

44. Poynter, J. N. *et al.* Statins and the Risk of Colorectal Cancer. *https://doi.org/10.1056/NEJMoa043792* **352**, 2184–2192 (2005).

Figure Legends:

Figure 1: Generation of a traceable mouse model of osteosarcoma cells.

(A) Schematic illustration of the experimental OS mouse model. **(B)** Genomic PCR confirming depletion of *Wwox* and Tr*p53* in the indicated genotypes. **(C)** Fluorescent microscope images demonstrating the expression of tdTomato reporter in the Osterix-expressing cells lining the bone. **(D)** Frozen bone sections representing the expression of tdTomato in the bone lining cells as well as in BM cells. **(E)** Flow cytometry analysis of BM cells demonstrating the presence of tdTomato positive cells in the Cre+ WT and DKO BM compared to the Cre- mice of similar age (2-months). **(F)** Immunoblot representing the deletion of WWOX and p53 in DKO BM cells compared to Cre+ WT BM cells (Quantification relative to Cre+ WT is represented under the blot). **WT**: Wildtype, **DKO**: Double Knock Out, **BF**: Bright Field, **RFP**: Red Fluorescent Protein, **BM**: Bone Marrow.

Figure 2: BM cells of OS-bearing mice are tumorigenic and exhibit metastatic ability.

(A) Flow cytometry analysis of tumor and paired BM cells (BMT) demonstrating comparable percentage of tdTomato expression (representative experiment-upper panel, average of the percentage of tdTomato positive cells from 14 mice-lower panel). **(B)** Colony formation assay of paired BMT and tumor cells indicating their survival capabilities compared to Cre+WT BM (representative images-left panel (Gimza stain and fluorescent microscope images), quantification of colony numbers of Cre+ BM, BMT and tumor cells-right panel (n=3). **(C)** Representative images of the OS tumors developed in NOD/SCID mice after intratibial (IT) injection of BMT and tumor cells compared to the control (Cre-BM cells)-upper panel, H&E validating the histological characteristics of OS, Immunofluorescence images representing the tdTomato positive cells in the developed tumors-lower panel. **(D)** Bar graph representing the percentage of immunocompromised mice that developed OS after IT injection of Cre-BM cells (Control), BMT and tumor cells. Histological validation reveals OS of osteoblastic type. **(E, F)** The migration and invasion ability respectively of tumor and BMT cells was determined using the wound-healing assay (IncuoCyte 96-well Scratch Wound Cell Migration/Invasion

assay). Time plot representing the relative wound density of tumor and BMT cells (n=3).

Figure 3: Molecular similarity between BMT and tumor cells.
(**A**) Principal component analysis (PCA) plot demonstrating clustering of tumor cells (n=3) with their paired BM cells (BMT) (n=3) away from control BM cells (n=4). **(B)** Venn diagram analysis revealing 164 of the genes are mutual between BMT and tumor cells. **(C)** Heat map representing the mutual genes between BMT and tumor cells clustering together away from the control BM cells. (**D**) Pathway enrichment analysis **(E)** Gene Set Enrichment Analysis (GSEA) of BMT and tumor cells demonstrating upregulation of cell cycle related pathways in both BMT and tumor cells including E2F and Myc targets.

Figure 4: young BM (yBM)-derived cells exhibit tumorigenic and metastatic ability.
(A) Summary graph of FACS experiments indicting the increase in the percentage of tdTomato positive cells in the genetically manipulated BM (DKO BM) cells but not in the wild type BM cells. **(B)** Colony formation assay of BM cells from young non-tumor bearing mice (n=9) reveals their survival and proliferation ability as compared to BM cells from Cre negative (n=3) and Cre+ WT (n=3) mice (Gimza stained colonies-left panel, fluorescent microscope images of the colonies-right panel, (n=9; 77.6±11.6). **(C)** Intratibial (IT)-injection of yBM cells develop OS tumors in immunocompromised mice after 3-4 months as validated by H&E. Immunofluorescence images representing the tdTomato positive cells in the developed tumors. **(D)** Bar graph representing the percentage of immunocompromised mice that developed OS following IT injection of tumor cells, and yBM cells, and resulted in histological fibroblastic/osteoblastic OS. **(E)** Fluorescent microscope images, tdTomato immunofluorescence and H&E staining representing lung metastasis in NOD/SCID mice after intravenous injection (IV) of yBM cells. **(F)** Bar graph representing the percentage of NOD/SCOD mice that developed lung metastasis after IV injection of yBM cells.

Figure 5: Early genes contributing to osteosarcomagenesis (yBM vs tumor cells and yBM vs BMT cells).

(**A**) Principal component analysis (PCA) plot demonstrating clustering of tumor cells (n=3) with *yBM* cells *at age of 1.5 months or 4-months were collected from tumor free mice* (n=6), away from control BM cells (n=4). **(B)** Venn diagram analysis revealing that 303 of the genes are mutual between yBM and tumor cells. **(C)** Pathway enrichment analysis demonstrating the upregulation of cell cycle related pathways in both yBM and tumor cells including E2F and Myc targets. (**D**) Principal component analysis (PCA) plot demonstrating clustering of yBM cells (n=6) with BMT cells (n=3) away from control BM cells (n=4). (**E**) Venn diagram representing the common and unique genes between yBM and BMT cells. **(F)** Pathway enrichment analysis demonstrating the upregulation of cell cycle related pathways in both yBM and BMT cells including E2F and Myc targets. **(G)** Gene Set Enrichment Analysis (GSEA) of yBM and tumor cells demonstrating upregulation of cell cycle related pathways including E2F and Myc targets. **(H)** GSEA of yBM and BMT cells demonstrating upregulation of cell cycle related pathways including E2F and Myc targets.

Figure 6: Early genes contributing to the tumorigenicity of DKO compared to SKO yBM cells.

(A) Venn diagram representing the common and unique genes between SKO and DKO yBM cells-left panel, Bar graph representing the significant pathways (Myc Targets) unique for DKO compared to SKO yBM-right panel. **(B)** Heat map showing the upregulation of Myc target genes in DKO-yBM (n=3) compared to SKO-yBM (n=3) cells. **(C)** Bar graph representing the upregulation of some Myc target genes (RNA sequencing data) in DKO compared to SKO yBM and control BM cells. **(D)** qPCR analysis validating the upregulation of Myc target genes in DKO compared to SKO yBM cells.

Figure 7: MCM7 Upregulation Promotes Tumor Progression.

(A) mRNA levels of MCM7 showing an upregulation in an age dependent manner compared to WT BM cells, ****p-value<0.0001. **(B)** Immunoblot validating

overexpression of endogenous MCM7 in yBM, BMT and tumor cells compared to WT BM, quantification of MCM7 protein levels relative to WT BM cells are shown- upper panel, immunoblot validating the decrease in the protein expression of c-Myc and MCM7 after Simvastatin (SVA) treatment-lower panel. **(C)** MTT assay demonstrating the dose dependent inhibitory effect of SVA on the proliferation of yBM, BMT and tumor cells but not on Cre+WT BM cells. **(D)** Colonogenic assay demonstrating the dose dependent inhibitory effect of SVA on the survival of yBM, BMT and tumor cells. **(E)** MTT assay demonstrating a significant dose dependent inhibitory effect of SVA on the proliferation of DKO compared to SKO yBM cells. **(F)** Average size and weight of the control or SVA (60mg/kg) treated tumors that developed in NOD/SCID mice after IT injection of yBM cells (* p-value <0.05, **p-value <0.01). **(G)** H&E staining of the Control and SVA treated tumors demonstrating the osteoblastic/fibroblastic characteristics of OS, IHC staining of MCM7 of the control and SVA treated tumors- left panel, quantification of the MCM7 positively stained nuclei demonstrating a significant reduction in the SVA treated tumors compared to the control- right panel (**p-value<0.001).

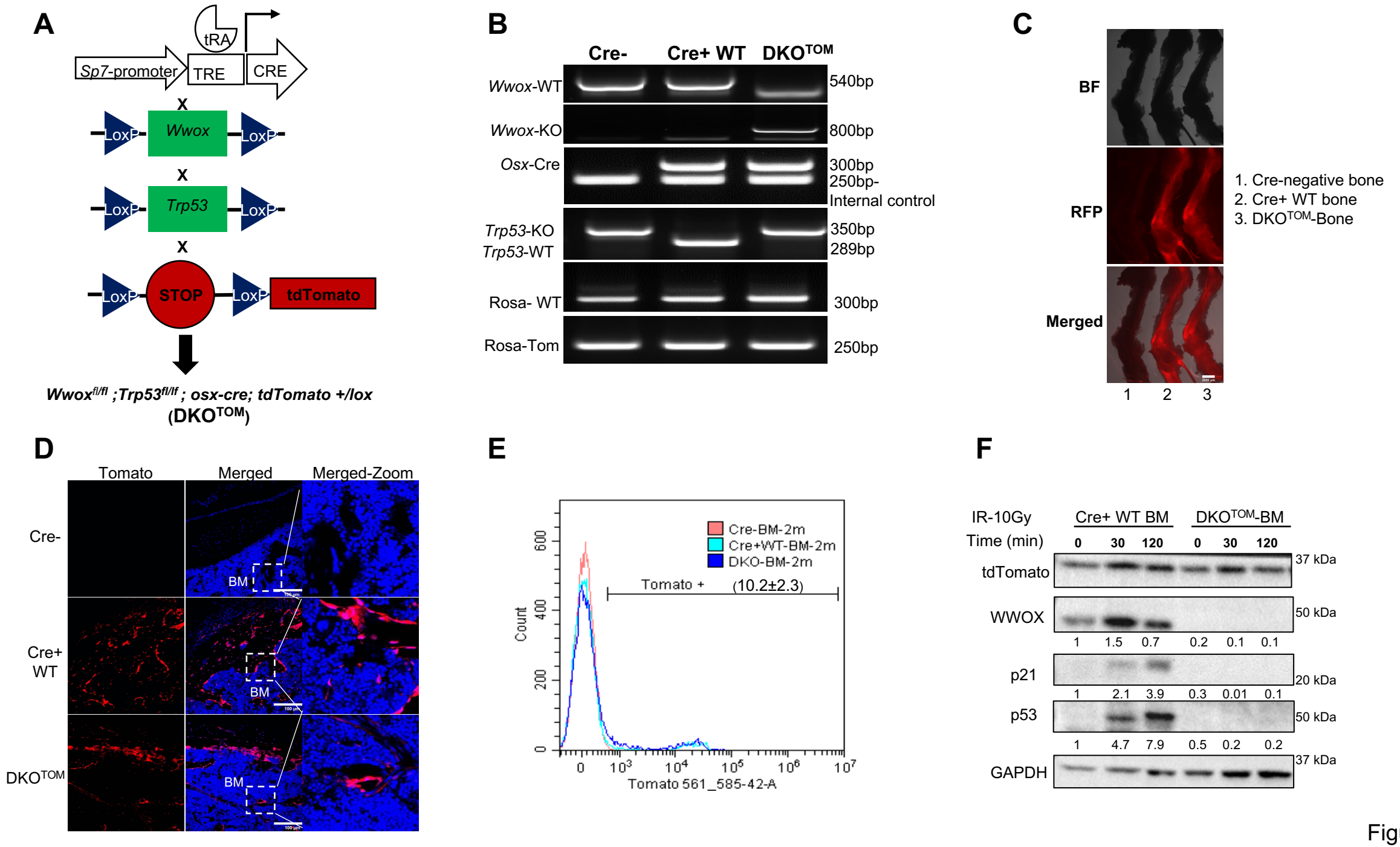
A
tRA
Sp7-promoter
TRE
CRE
X
LoxP
Wwox
LoxP
X
LoxP
Trp53
LoxP
X
LoxP
STOP
LoxP
tdTomato
Wwox fl/fl ;Trp53 fl/lf ; osx-cre; tdTomato +/lox
(DKO TOM)
B
Cre-
Cre+ WT
DKO TOM
Wwox-WT
540bp
Wwox-KO
800bp
Osx-Cre
300bp
250bp-
Internal control
Trp53-KO
Trp53-WT
350bp
289bp
Rosa- WT
300bp
Rosa-Tom
250bp
C
BF
RFP
Merged
1. Cre-negative bone
2. Cre+ WT bone
3. DKO TOM-Bone
1
2
3
D
Tomato
Merged
Merged-Zoom
Cre-
Cre+
WT
DKO TOM
BM
E
Cre-BM-2m
Cre+WT-BM-2m
DKO-BM-2m
Tomato +
(10.2±2.3)
Count
Tomato 561_585-42-A
F
IR-10Gy
Time (min)
Cre+ WT BM
DKO TOM-BM
0
30
120
tdTomato
37 kDa
WWOX
50 kDa
1
1.5
0.7
0.2
0.1
0.1
p21
20 kDa
1
2.1
3.9
0.3
0.01
0.1
p53
50 kDa
1
4.7
7.9
0.5
0.2
0.2
GAPDH
37 kDa

Figure 1

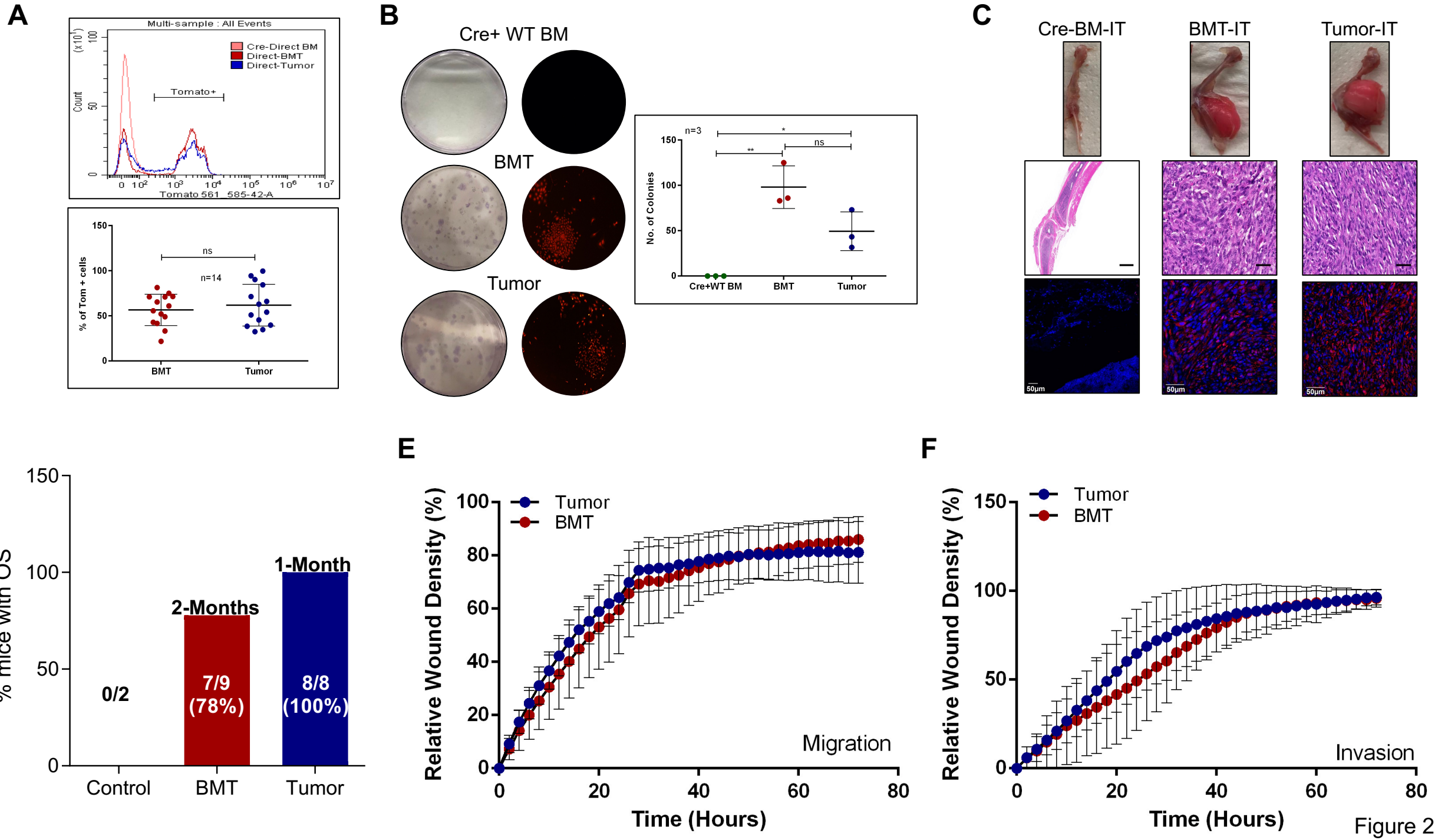
A
Multi-sample : All Events
Cre-Direct BM
Direct-BMT
Direct-Tumor
Tomato+
Count
Tomato 561 585-42-A
% of Tom + cells
ns
n=14
BMT
Tumor
B
Cre+ WT BM
BMT
Tumor
n=3
No. of Colonies
Cre+WT BM
BMT
Tumor
C
Cre-BM-IT
BMT-IT
Tumor-IT
50µm
D
% mice with OS
0/2
2-Months
7/9 (78%)
1-Month
8/8 (100%)
Control
BMT
Tumor
E
Relative Wound Density (%)
Tumor
BMT
Migration
Time (Hours)
F
Relative Wound Density (%)
Tumor
BMT
Invasion
Time (Hours)

Figure 2

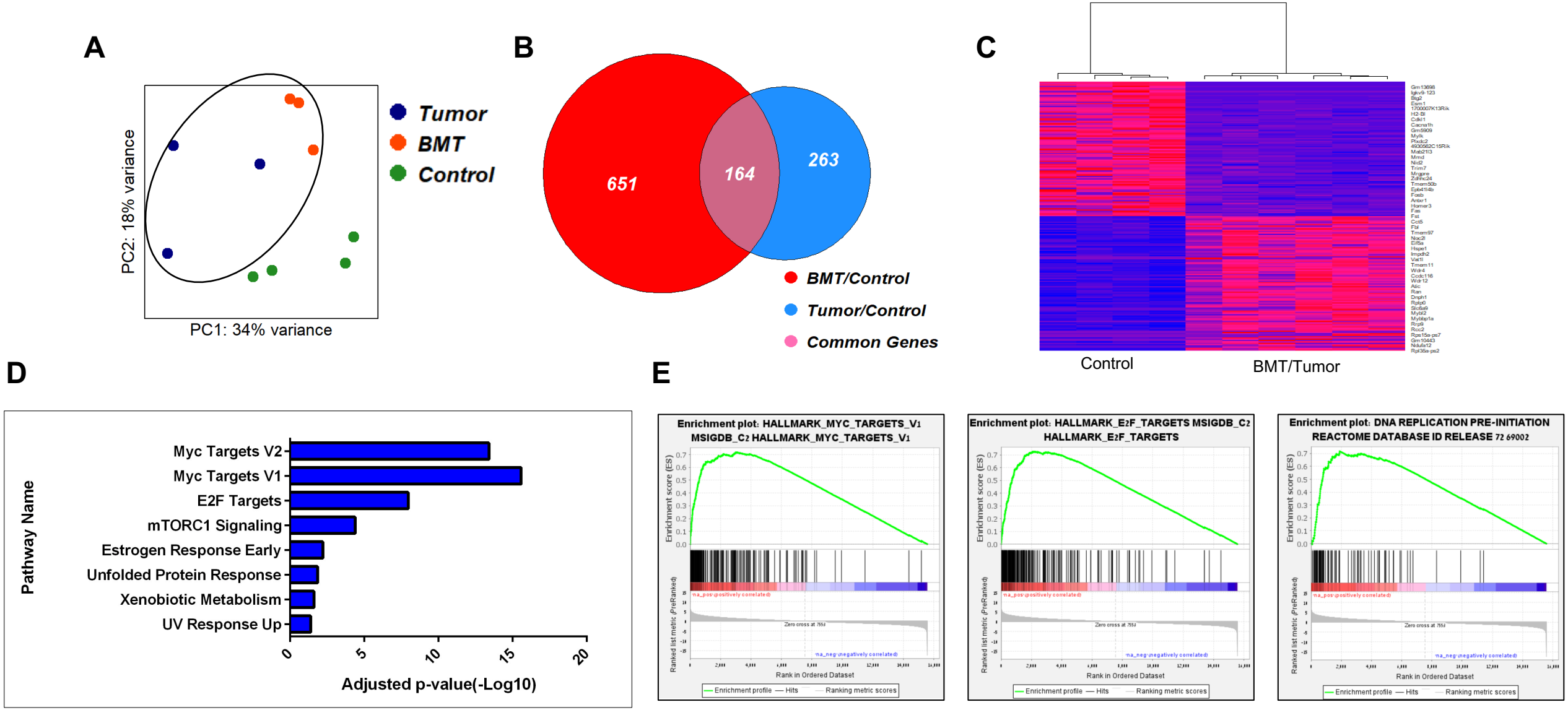
A
PC2: 18% variance
PC1: 34% variance
Tumor
BMT
Control
B
651
164
263
BMT/Control
Tumor/Control
Common Genes
C
Control
BMT/Tumor
D
Pathway Name
Myc Targets V2
Myc Targets V1
E2F Targets
mTORC1 Signaling
Estrogen Response Early
Unfolded Protein Response
Xenobiotic Metabolism
UV Response Up
0
5
10
15
20
Adjusted p-value(-Log10)
E
Enrichment plot: HALLMARK_MYC_TARGETS_V1
MSIGDB_C2 HALLMARK_MYC_TARGETS_V1
Enrichment plot: HALLMARK_E2F_TARGETS MSIGDB_C2
HALLMARK_E2F_TARGETS
Enrichment plot: DNA REPLICATION PRE-INITIATION
REACTOME DATABASE ID RELEASE 72 69002
Enrichment score (ES)
Ranked list metric (PreRanked)
Rank in Ordered Dataset
Enrichment profile
Hits
Ranking metric scores

Figure 3

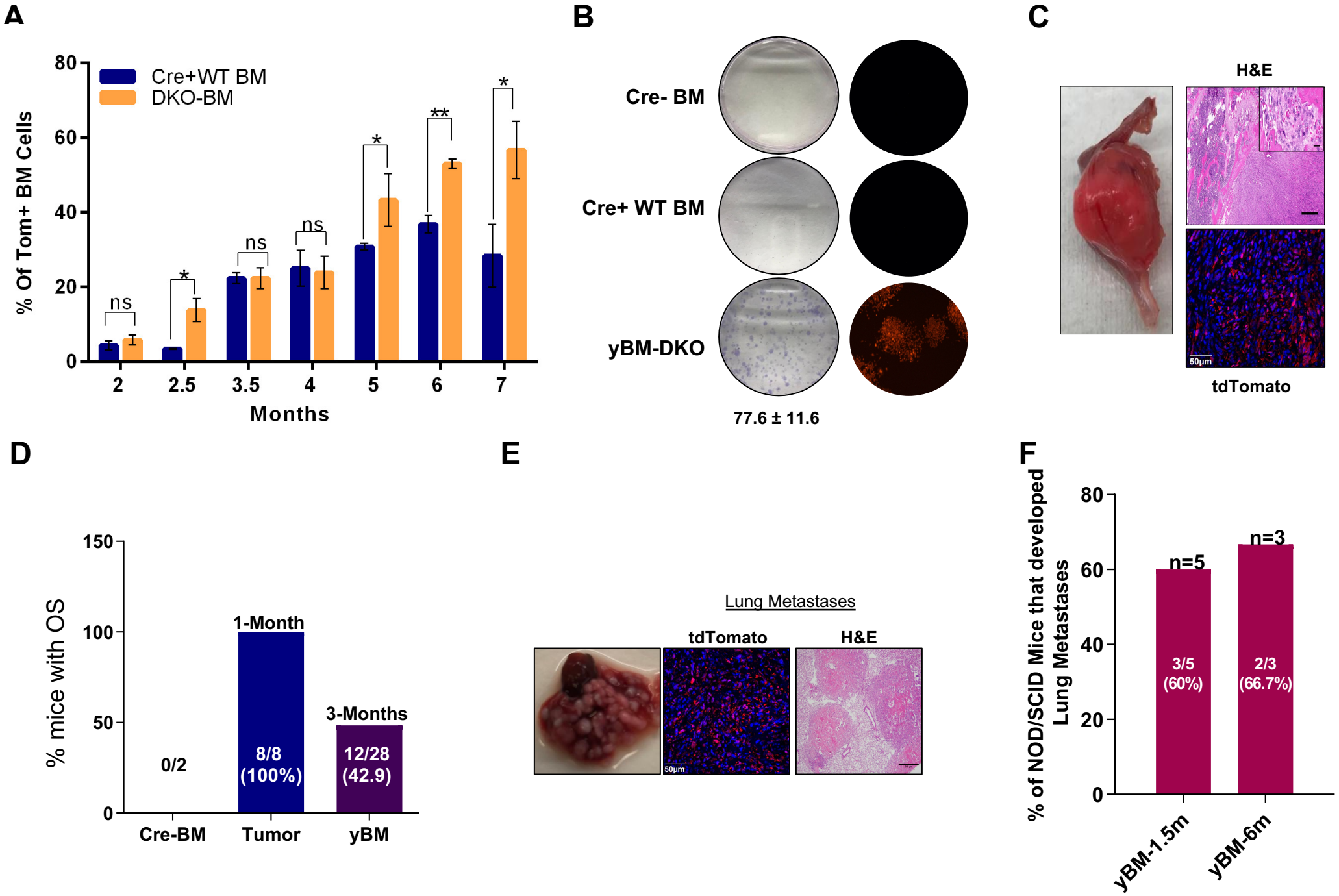
A
Cre+WT BM
DKO-BM
% Of Tom+ BM Cells
80
60
40
20
0
ns
*
ns
ns
*
**
*
2
2.5
3.5
4
5
6
7
Months
B
Cre- BM
Cre+ WT BM
yBM-DKO
77.6 ± 11.6
C
H&E
50µm
tdTomato
D
% mice with OS
150
100
50
0
0/2
1-Month
8/8
(100%)
3-Months
12/28
(42.9)
Cre-BM
Tumor
yBM
E
Lung Metastases
tdTomato
H&E
50µm
F
% of NOD/SCID Mice that developed Lung Metastases
80
60
40
20
0
n=5
n=3
3/5
(60%)
2/3
(66.7%)
yBM-1.5m
yBM-6m

Figure 4

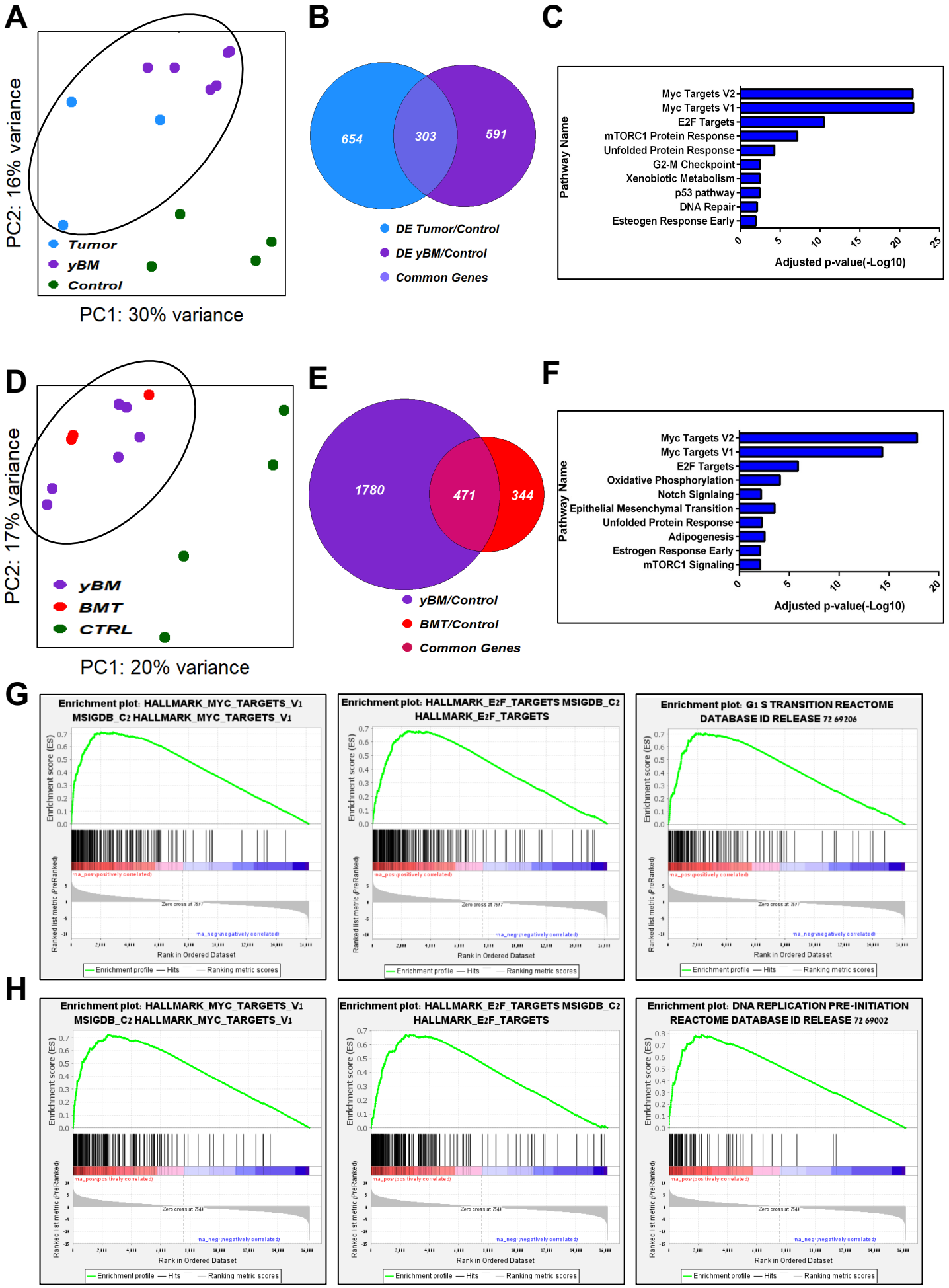
A
PC2: 16% variance
PC1: 30% variance
Tumor
yBM
Control
B
654
303
591
DE Tumor/Control
DE yBM/Control
Common Genes
C
Pathway Name
Myc Targets V2
Myc Targets V1
E2F Targets
mTORC1 Protein Response
Unfolded Protein Response
G2-M Checkpoint
Xenobiotic Metabolism
p53 pathway
DNA Repair
Esteogen Response Early
Adjusted p-value(-Log10)
D
PC2: 17% variance
PC1: 20% variance
yBM
BMT
CTRL
E
1780
471
344
yBM/Control
BMT/Control
Common Genes
F
Pathway Name
Myc Targets V2
Myc Targets V1
E2F Targets
Oxidative Phosphorylation
Notch Signlaing
Epithelial Mesenchymal Transition
Unfolded Protein Response
Adipogenesis
Estrogen Response Early
mTORC1 Signaling
Adjusted p-value(-Log10)
G
Enrichment plot: HALLMARK_MYC_TARGETS_V1 MSIGDB_C2 HALLMARK_MYC_TARGETS_V1
Enrichment plot: HALLMARK_E2F_TARGETS MSIGDB_C2 HALLMARK_E2F_TARGETS
Enrichment plot: G1 S TRANSITION REACTOME DATABASE ID RELEASE 72 69206
Enrichment score (ES)
Ranked list metric (PreRanked)
Rank in Ordered Dataset
Enrichment profile
Hits
Ranking metric scores
H
Enrichment plot: HALLMARK_MYC_TARGETS_V1 MSIGDB_C2 HALLMARK_MYC_TARGETS_V1
Enrichment plot: HALLMARK_E2F_TARGETS MSIGDB_C2 HALLMARK_E2F_TARGETS
Enrichment plot: DNA REPLICATION PRE-INITIATION REACTOME DATABASE ID RELEASE 72 69002
Enrichment score (ES)
Ranked list metric (PreRanked)
Rank in Ordered Dataset
Enrichment profile
Hits
Ranking metric scores

Figure 5

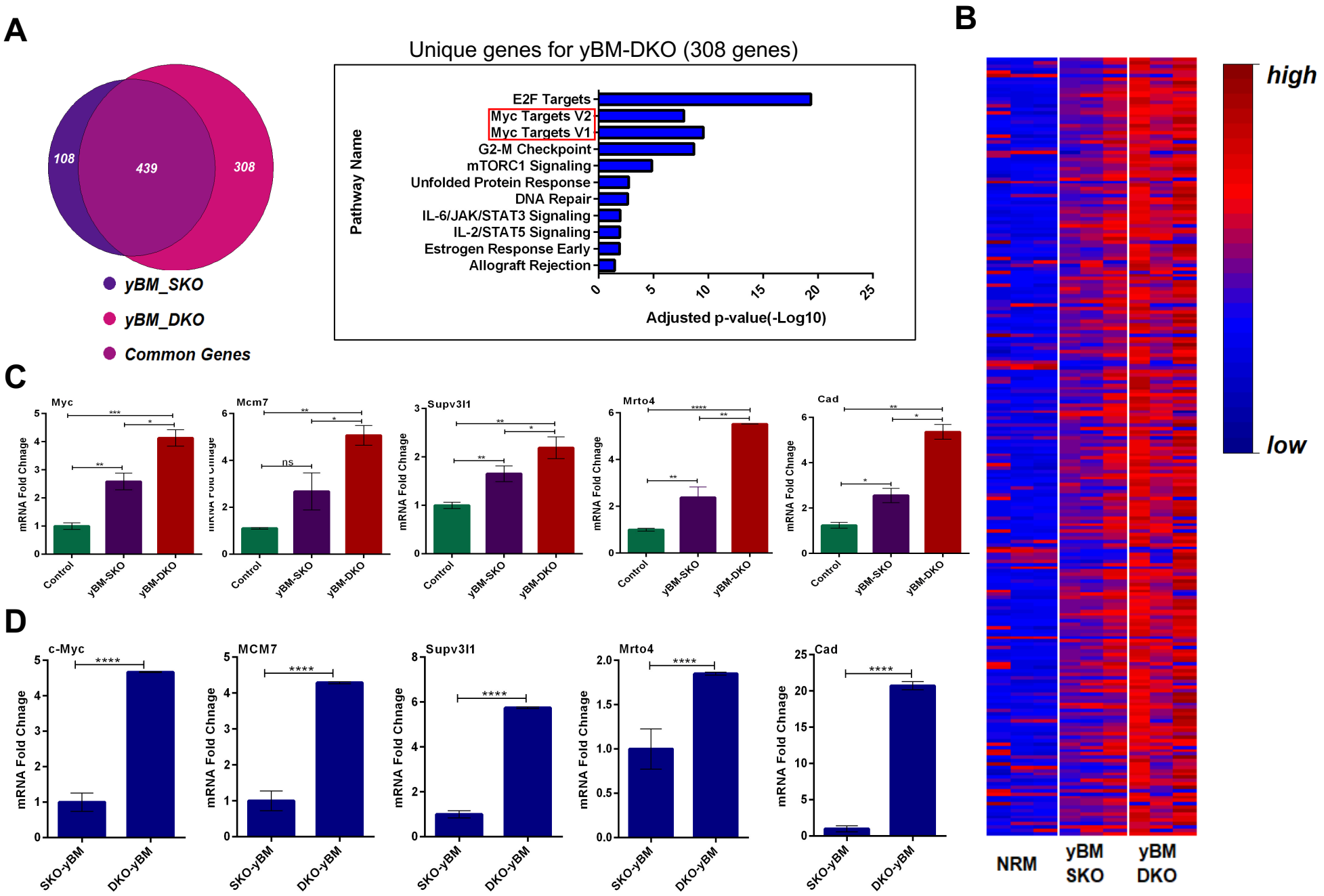
A
108
439
308
yBM_SKO
yBM_DKO
Common Genes
Unique genes for yBM-DKO (308 genes)
Pathway Name
E2F Targets
Myc Targets V2
Myc Targets V1
G2-M Checkpoint
mTORC1 Signaling
Unfolded Protein Response
DNA Repair
IL-6/JAK/STAT3 Signaling
IL-2/STAT5 Signaling
Estrogen Response Early
Allograft Rejection
0
5
10
15
20
25
Adjusted p-value(-Log10)
B
high
low
NRM
yBM SKO
yBM DKO
C
Myc
Mcm7
Supv3l1
Mrto4
Cad
mRNA Fold Chnage
Control
yBM-SKO
yBM-DKO
ns
D
c-Myc
MCM7
Supv3l1
Mrto4
Cad
mRNA Fold Chnage
SKO-yBM
DKO-yBM

Figure 6

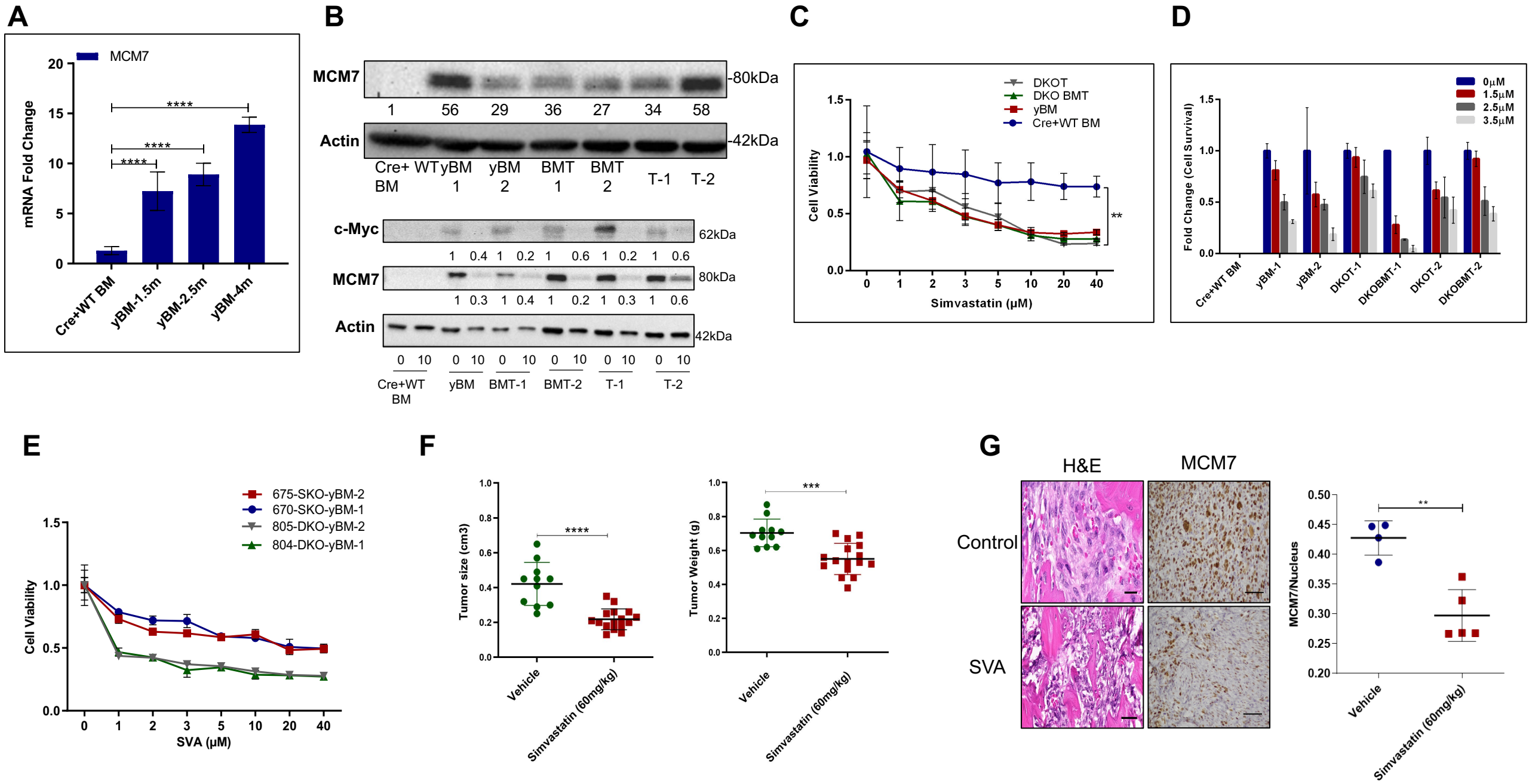
A
MCM7
mRNA Fold Change
****
****
****
Cre+WT BM
yBM-1.5m
yBM-2.5m
yBM-4m
B
MCM7
-80kDa
1 56 29 36 27 34 58
Actin
-42kDa
Cre+ WT BM
yBM 1
yBM 2
BMT 1
BMT 2
T-1
T-2
c-Myc
62kDa
1 0.4 1 0.2 1 0.6 1 0.2 1 0.6
MCM7
80kDa
1 0.3 1 0.4 1 0.2 1 0.3 1 0.6
Actin
42kDa
0 10 0 10 0 10 0 10 0 10 0 10
Cre+WT BM
yBM
BMT-1
BMT-2
T-1
T-2
C
DKOT
DKO BMT
yBM
Cre+WT BM
Cell Viability
Simvastatin (μM)
**
D
0μM
1.5μM
2.5μM
3.5μM
Fold Change (Cell Survival)
Cre+WT BM
yBM-1
yBM-2
DKOT-1
DKOBMT-1
DKOT-2
DKOBMT-2
E
675-SKO-yBM-2
670-SKO-yBM-1
805-DKO-yBM-2
804-DKO-yBM-1
Cell Viability
SVA (μM)
F
Tumor size (cm3)
****
Vehicle
Simvastatin (60mg/kg)
Tumor Weight (g)
***
Vehicle
Simvastatin (60mg/kg)
G
H&E
MCM7
Control
SVA
MCM7/Nucleus
**
Vehicle
Simvastatin (60mg/kg)

Figure 7